PERGAMON

Journal of Structural Geology 24 (2002) 953–962

JOURNAL OF STRUCTURAL GEOLOGY

www.elsevier.com/locate/jstrugeo

The influence of backstop dip and convergence velocity in the growth of viscous doubly-vergent orogenic wedges: insights from thermomechanical laboratory experiments

Federico Rossetti[a,*], Claudio Faccenna[a], Giorgio Ranalli[b]

[a]*Dipartimento di Scienze Geologiche, Università "Roma Tre", Largo S.L. Murialdo 1, 00146 Rome, Italy*
[b]*Department of Earth Sciences and Ottawa-Carleton Geoscience Centre, Carleton University, Ottawa, Canada K1S 5B6*

Received 12 February 2001; revised 25 August 2001; accepted 29 August 2001

Abstract

We investigate the effects of convergence velocity and backstop geometry on the evolution of experimental viscous doubly-vergent orogenic wedges. Experiments are performed in a thermomechanical shortening box, using the Newtonian properties of 52/54 EN type paraffin as analogue to the natural strength distribution in the continental crust. A velocity discontinuity is imposed at the subduction slot, where the base plate is pulled below a rigid backstop. The mobile base plate dips 5°. Two different backstop dips (60° and 30°) are used in combination with constant convergence velocities of 2 and 10 cm h^{-1}. Results point out that backstop geometry exerts a first-order control on the evolution of doubly-vergent experimental wedges. Steeply-dipping backstops cause the stationary uplift of the wedge axial region above the subduction slot, whereas shallow-dipping backstops allow its retroward translation, in concomitance with a more pronounced deformation in the retrowedge. Convergence velocity controls the uplift in the wedge axial region and the amount of the outward migration of the deformation front in both the prowedge and retrowedge regions. For fast convergence velocity and shallow-dipping backstop, deformation in the retrowedge is favoured. An increase in the backstop dip and/or a decrease in the convergence velocity favour deformation in the prowedge. Both prowedge and retrowedge tend to grow in self-similar conditions, with an aspect ratio depending upon the backstop dip and convergence velocity. These results may have important consequences for the evolution and deformation style of ductile-dominated orogenic wedges, suggesting that location of the axial region and deformation progression in natural orogens can be strongly controlled by boundary and kinematic conditions.

Keywords: Analogue modelling; Orogenic wedges; Backstop dip; Convergence velocity

1. Introduction

Doubly-vergent orogenic wedges have been commonly described both in fossil and active examples of convergent margins and continental collision zones, such as the Alps (e.g. Argand, 1911; Polino et al., 1990; Schmidt et al., 1996; Escher and Beaumont, 1997 and references therein), the Andes (e.g. Molnar and Lyon-Caen, 1988; Adam and Reuther, 2000; Toboaga et al., 2000), the Pyrenees (Muñoz, 1992), the Apennines (Principi and Treves, 1984; Jolivet et al., 1998), the Atlas Mountains of Morocco (Beauchamp et al., 1999), the South Island of New Zealand (Koons, 1990), and a variety of forearcs (Silver and Reed, 1989). Many numerical (e.g. Braun, 1993; Willett et al., 1993; Beaumont et al., 1994; Beaumont and Quinlan, 1994; Batt and Braun, 1997; Willet, 1999), analytical (e.g. Stockmal, 1983; Dahlen, 1990) and analogue (e.g. Davis et al., 1983; Malavieille, 1984; Byrne et al., 1988; Merle and Guiller, 1989; Koons, 1990; Wang and Davis, 1996; Storti et al., 2000) studies have shown that crustal shortening is accommodated through the formation of a doubly-vergent orogenic wedge, whose geometry and evolution is controlled by both the internal and basal décollement strengths. In doubly-vergent orogens, the backstop represents the stronger, relatively undeformed region in the hinterland of orogenic wedges against which the material accumulates during shortening (Byrne et al., 1993). The backstop may be composed of crystalline rocks or previously accreted material, and both hinterland- (type I of Byrne et al., 1993) and foreland- (type II of Byrne et al., 1993) dipping backstops have been described (e.g. Byrne et al., 1988; Silver and

* Corresponding author. Tel.: +39-06-548-88043; fax: +39-06-548-88201.
E-mail address: rossetti@uniroma3.it (F. Rossetti).

0191-8141/02/$ - see front matter
PII: S0191-8141(01)00127-4

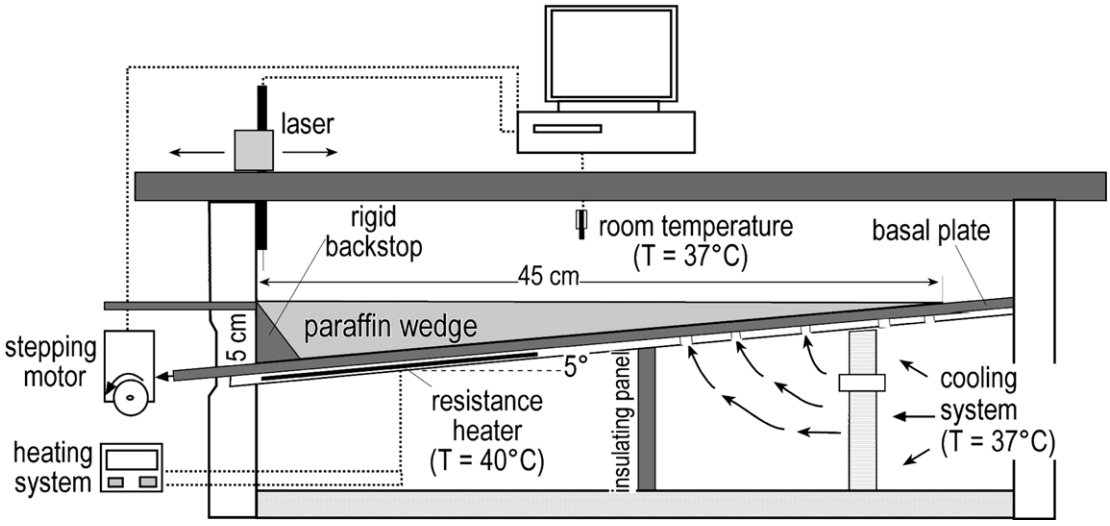

Fig. 1. Schematic drawing of the experimental apparatus (modified after Rossetti et al., 2001). The experimental set-up includes a 3°C temperature gradient from the base plate to the top of the model and from the back to the front of the model. The accuracy of temperature control is ±0.2–0.3°C. A rigid backstop is placed at the rear of the paraffin wedge.

Reed, 1988; Torrini and Speed, 1989; Von Huene and Scholl, 1991). Analogue, analytical and numerical models of the role of backstop in the evolution of orogenic wedges may be classified into two main categories: (i) indentor or backstop models, in which a rigid, variably inclined wall is moved laterally to cause contraction in the upper plate (e.g. Mulugeta, 1988; Dahlen, 1990; Colletta et al., 1991; Marshak and Wilkerson, 1992; Koyi, 1995; Bonini et al., 1999); and (ii) traction-reversal models, in which traction applied at the base of the upper plate by the subducting plate produces conjugate dipping shear zones resulting in an asymmetric pair of contractional wedges (e.g. Davis et al., 1983; Stockmal, 1983; Malavieille, 1984; Koons, 1990; Braun, 1993; Byrne et al., 1993; Willett et al., 1993; Beaumont and Quinlan, 1994; Wang and Davis, 1996; Willett, 1999; Storti et al., 2000). Within the latter model framework, the mechanical (wedge buttressing; Byrne et al., 1988, 1993; Lallemand et al., 1992) versus geometrical (consequence of the kinematics of the plate boundary; Malavielle, 1984; Willett et al. 1993; Buck and Sokoutis, 1994; Willett, 1999; Storti et al., 2000) role of backstop in the evolution of the orogenic wedges is still under debate (see e.g. Davis, 1996; Beaumont et al., 1999).

In this paper we present a set of thermomechanical viscous laboratory experiments addressed to study the sequential growth of viscous orogens during accretion against a rigid, foreland-dipping backstop and development of doubly-vergent wedges. The growth of the model wedges is examined as a function of different backstop configurations and applied convergence velocities. We find that these parameters play a fundamental role in determining the shape, uplift rate and deformation style of the model wedges, bearing important implications for the large-scale evolution of viscous orogens.

2. Modelling set-up

The depth-dependent rheological stratification of the continental crust, from pressure-dependent, temperature-independent Coulomb behaviour to approximately pressure-independent, temperature-dependent ductile behaviour (e.g. Ranalli and Murphy 1987; Ord and Hobbs, 1989; Kohlstedt et al., 1995; Ranalli, 1995), represents the major limitation for the applicability of both the uniform plasticity critical taper theory and sandbox techniques to model the large-scale evolution of viscous orogenic wedges. Properly scaled analogue modelling of large-scale orogenic accretion should thus account for the variations in rheological properties induced by the temperature profile within the growing orogenic wedge (e.g. Pavlis and Bruhn, 1983; Platt, 1986; Jamieson and Beaumont, 1988; Barr and Dahlen, 1989).

In order to model the evolution of viscous orogenic wedges, we treat the crust as a material with a Newtonian viscosity varying with depth (temperature) (Rossetti et al., 2000; 2001). This approach is similar to the ones used in previous numerical, analytical, and analogue studies, where both uniform (e.g. Emerman and Turcotte, 1983; Buck and Sokoutis, 1994; Allemand and Lardeaux, 1997; Willett, 1999), and variable (Royden, 1996) viscosity settings have been used as analogue to the strength distribution within the continental crust.

The temperature-dependent variation in viscosity of commercial 52/54 EN type paraffin (Newtonian flow conditions for $T \geq 37$°C) is used as analogue to crustal ductility (Rossetti et al., 1999). Paraffin is deformed in the thermomechanical shortening machine described in Rossetti et al. (2000; 2001), adapted to reproduce the geometrical conditions and kinematics of accretion along a type-II backstop (Fig. 1). This allows us to reproduce the strength gradient within the continental crust below the brittle–ductile

Table 1
Physical parameters used in this study and scaling factors between nature (N) and model (M) (after Rossetti et al., 2000; 2001)

Parameter	Unit	Nature (N)	Model (M)	Scaling factor (N/M)
Length (l)	m	3×10^{4}[a,b]	5×10^{-2}	6×10^{5}
Density (ρ)	kg m^{-3}	2500	850	2.9
Gravity acceleration (g)	m s^{-2}	9.8	9.8	1
Stress (ρgl) (σ)	Pa	7.5×10^{8}	4.2×10^{2}	1.8×10^{6}
Thermal diffusivity (k)	m^2 s^{-1}	10^{-6}[c]	8×10^{-8}	1.2×10^{-3}
Reference time (l^2/k) (t)	s	9×10^{14}	3×10^{4}	3×10^{10}
Viscosity (η)	Pa s	10^{21}–10^{17}[a,d]	10^{7}–10^{5}	10^{14}–10^{12}
Activation energy (E)	kJ mol^{-1}	200[d]	900	0.2

[a] Pavlis and Bruhn (1983).
[b] Barr and Dahlen (1989).
[c] Davy and Cobbold (1991).
[d] Ranalli (1995).

transition. The experimental apparatus consists of a 75 cm long, 40 cm wide and 50 cm high plexiglas box, located inside an insulated room maintained at a constant temperature of 37°C. The mobile basal plate is thermally conductive and may be inclined at various angles. A resistance heater is positioned below the basal plate, settled to a temperature of 40°C. The displacement is applied by means of a screw jack, fixed onto the basal plate and connected to a stepping motor. A displacement transducer reveals the incremental strain. Paraffin is contained inside the box and the movement of the basal plate forces it to flow against the rigid backstop, simulating the accretion of material during subduction.

The experimental arrangement establishes a 3°C temperature gradient (from 37 to 40°C) both along the vertical and the base plate of the paraffin experimental wedge, simulating the distribution of temperature in natural wedges. Table 1 shows the mean scaling factors between the natural prototype and the model wedges. The corresponding viscosity (strength) structure in the model wedge is shown in Fig. 2: it consists of a thin upper layer of uniform viscosity and a lower layer where viscosity decreases with depth (temperature). Temperature is not considered in the scaling procedure; it constitutes a controlling factor to obtain mechanical similarity between model and nature. For the imposed 3°C temperature increase, using an experimental strain rate in the order of 10^{-5}–10^{-6} s^{-1}, viscosity values of paraffin are associated with a flow stress drop of two orders of magnitude (from 100 to 1 Pa) (Fig. 2). The corresponding stress values for the natural prototype as defined by the stress scale (10^6) vary from 100 to 1 MPa. These values are in good agreement with the creep strength values of crustal rocks at temperatures above the brittle–ductile transition (Rossetti et al., 1999).

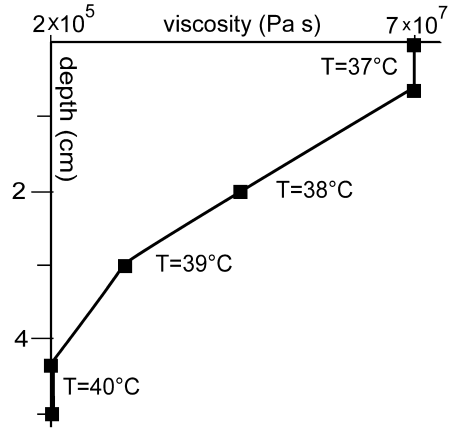

Fig. 2. Initial viscosity structure as function of depth (temperature) within the model wedge (after Rossetti et al., 2000). The upper layer has a constant viscosity and is underlain by a lower layer where viscosity decreases with depth.

Our experimental set-up does not allow for the simulation of a thick brittle layer. Finite strength is modelled only qualitatively by a uniform viscosity upper layer (see also Royden, 1996), which is stronger with respect to the underlaying weaker layer in which strength decreases with depth. This represents an oversimplification of the rheological stratification of the continental crust, but it has the advantage of providing first-order insights into the relationship between the strength distribution in the crust and the large-scale crustal deformation (e.g. Royden, 1996). The modelling technique, in fact, scales correctly the depth dependence of viscosity (strength) in the ductile parts of the wedge. Our models, therefore, simulate the large-scale evolution of orogenic wedges which, because of their size and/or thermal conditions, can be assumed to exhibit predominantly viscous behaviour.

The experimental set-up and the thermal scaling of the models are adequate when advection predominates over conduction in controlling the thermal structure of the wedge. This is in good accordance with the analytical and numerical simulation of temperature structure of convergent plate margins, where the downward advection of cold oceanic lithosphere dominates the thermal structure of subduction zones (e.g. Wang and Shi, 1984; Davy and Gillet, 1986; Peacock, 1996 and references therein).

In the experiments described in this paper, the mobile basal plate dips at an angle β of 5°. A velocity discontinuity is imposed at the subduction slot S, where the basal plate is

Table 2
Experimental configurations and velocities

Experiment	Backstop dip	Convergence velocity	h (cm)	L_0 (cm)
W98-01	60°	10 cm h^{-1}	5.5	39
W98–02	60°	2 cm h^{-1}	5.5	39
W98–03	30°	10 cm h^{-1}	5.0	45
W98–04	30°	2 cm h^{-1}	5.0	45

pulled below the rigid backstop (Fig. 1). In order to model the simplest configuration, the subduction slot is fixed, not incorporating the effects of dynamic motion of the subduction zones. The traction reversal model is thus adopted and accretion occurs with a rigid backstop. No subduction channel is present. Our experimental configuration thus basically follows the sandbox modelling of Davis et al. (1983), Byrne et al. (1988) and Lallemand et al. (1992). Two different dipping backstop configurations are used, 30° and 60° (measured clockwise from the mobile basal plate). Two sets of experiments are presented for constant convergence velocity equal to 10 cm h^{-1} (bulk shortening rate of 5×10^{-5} s^{-1}) and 2 cm h^{-1} (bulk shortening rate of 10^{-5} s^{-1}), respectively (Table 2). Equal amounts of total shortening (40%) are used in each experiment.

Model topographies are monitored at constant time lapse with a laser scan machine (resolution of the order of 100 μm) running over the model parallel to the shortening direction. These data are recorded as data file to obtain variations in the model topography through time. Line drawing of the evolution (every 5% shortening) of the models permits measurements of a number of key parameters for the quantitative analysis of the experiments. Each model was repeated twice to check reproducibility of results.

3. Model parameters

Our experimental wedges grow through the development of two deforming regions facing opposite directions. We adopt the nomenclature of Willett et al. (1993), defining the 'prowedge' as the deforming region on the incoming side of the subduction zone and 'retrowedge' the deforming region on the side of the overriding plate, whereas the axial zone is the central region between them (Fig. 3). The parameters h', l, and β represent the initial wedge height, the vertical height of the backstop ($h = h'$ in these experiments), the shortening along the base plate, and the angle of dip of the base plate, respectively. For each step of our experiments we measure the following parameters (Fig. 3): (i) the height of the wedge (H), measured at the inflexion point of the axial zone with respect to the subduction slot (S); (ii) the uplift of wedge axial zone (u), defined as $H - h$; (iii) the uplift of the retrowedge (u_r), defined as $u_r = H - h'$; (iv) the uplift of prowedge (u_p), defined as $u_p = u_r + l\sin\beta$; (v) the position (p) of the wedge axial zone with respect to the subduction slot; (vi) the distance, measured along a horizontal plane corresponding to the top of the undeformed wedge, of the outer deformation fronts from the wedge axial zone region for both the prowedge (L_p) and the retrowedge (L_r); and (vii) the total length of the wedge, defined as $L_{tot} = L_p + L_r$. The determination of these parameters allows characterisation of the overall evolution of the model wedges as a function of both backstop configuration and applied convergence velocity. Particularly, the ratios of u_p/L_p and u_r/L_r provide information on the overall wedge evolution, indicating the differential contribution of uplift and horizontal propagation of the deformation in the prowedge and retrowedge regions, respectively. These ratios correspond to the aspect ratio A as defined in Rossetti et al. (2000; 2001) for the 90°-dipping backstop configurations.

4. Results of the laboratory experiments

We select four out of 12 experiments to show the influence of backstop geometry and convergence velocity on the shape and growth of model wedges. Fig. 4 compares the topographic profiles for the two backstop configurations. In all the models we observe a similar evolutionary path, characterised by the formation of a topographic high and, afterwards, by a synchronous outward propagation of the deformation front in both the pro- and retrowedge regions. The position of the wedge axial zone and the propagation of the deformation fronts is strictly controlled by both backstop dip and applied convergence velocity and will be described in the following sections.

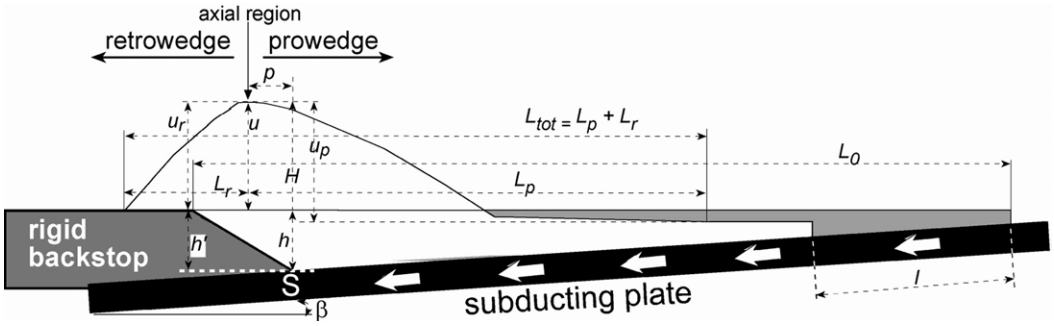

Fig. 3. Reference geodynamic model and parameters measured in the experimental wedges.

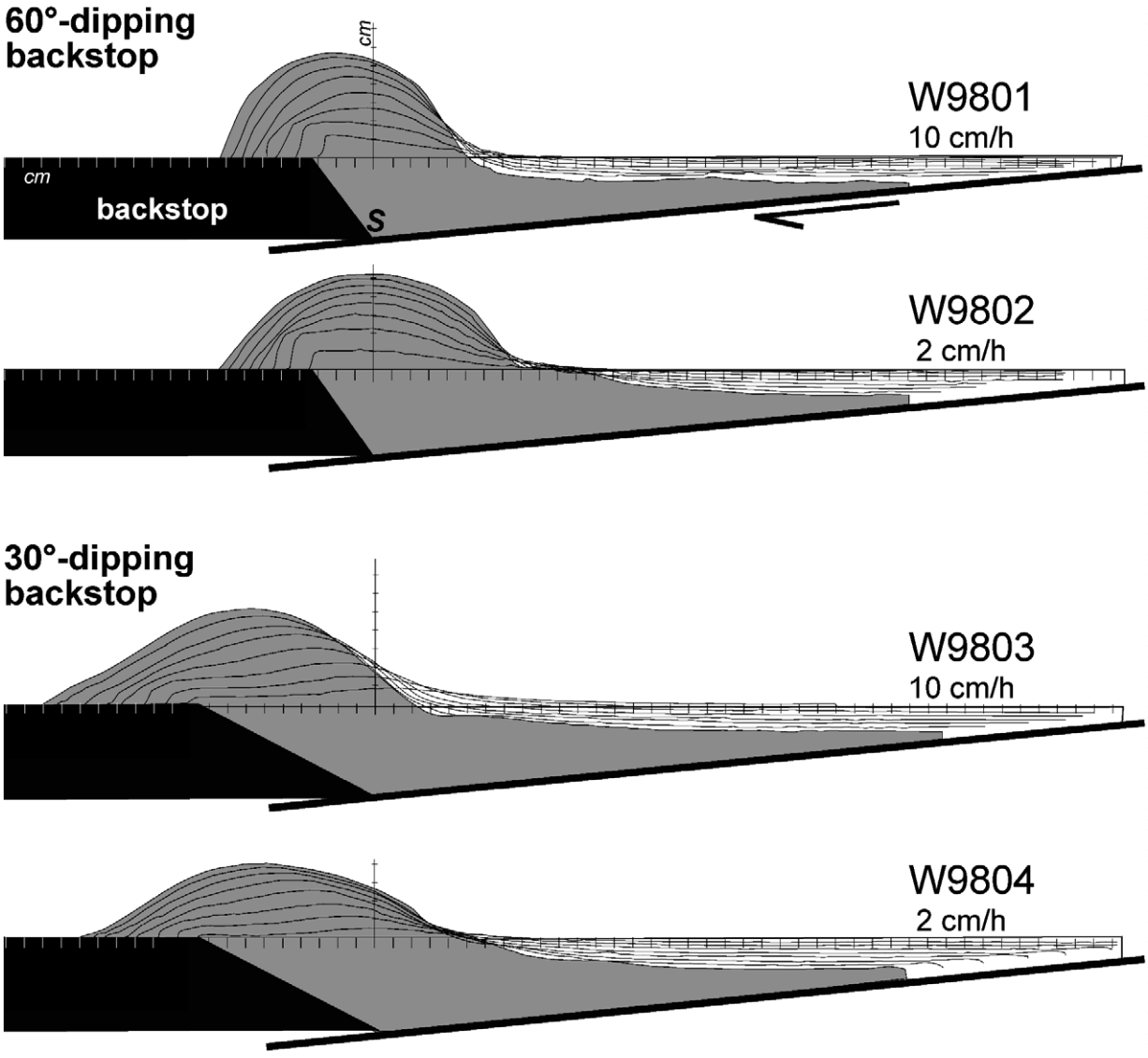

Fig. 4. Laser-acquired topographic profiles for each experiment (see text for further details).

4.1. 60°-dipping backstop configuration (experiments W9801 and W9802)

The position of the uplifted plug in the early stages of shortening is controlled by the convergence velocity. For fast convergence velocity the wedge axial zone culmination forms nearly above the backstop culmination, whereas it forms closer to the subduction slot for the slow convergence velocity (Fig. 4). With increasing shortening, the position of the wedge axial zone remains fixed for low convergence velocity and only a low retroward migration is observed for fast convergence velocity (Fig. 5). The convergence velocity has only minor control on the amount of uplift in the wedge axial region, even if the highest values are obtained for the fast convergence velocity (Fig. 6). Conversely, the influence of convergence velocity is clearly shown in Fig. 7a by plotting u_p/L_p and u_r/L_r with increasing shortening. Higher values characterise the fast convergence

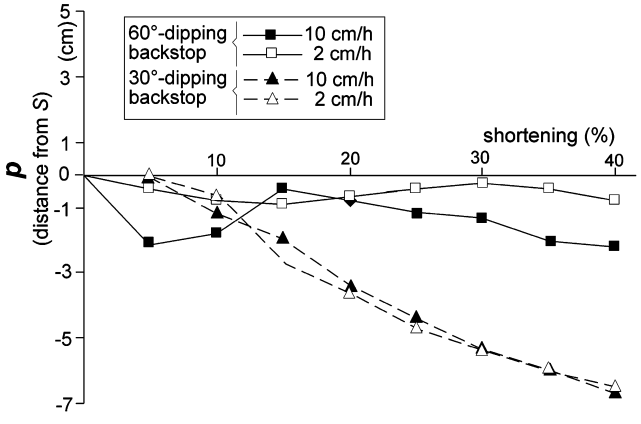

Fig. 5. Migration of the axial zone (negative values toward the retrowedge) with respect to the subduction slot.

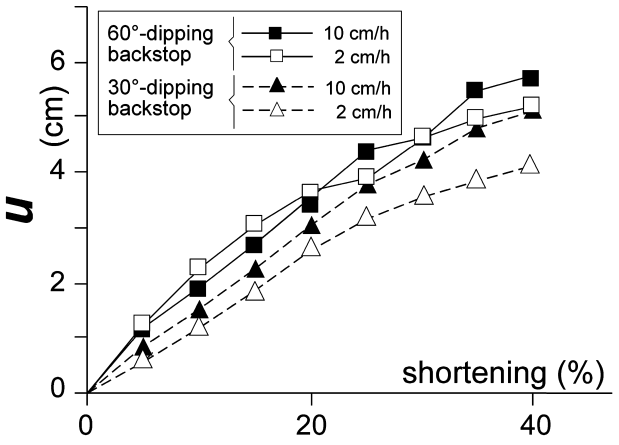

Fig. 6. Plots of uplift of the wedge axial zone (u), measured respect to the initial topography, vs. % shortening for the different experimental configurations.

velocity, with a final equilibrium condition (constant ratio between uplift in the axial region and length of the deformed area) for both the prowedge (at 30% shortening) and retrowedge (at 30% shortening) at values of 0.60 and 0.80, respectively. Lowering the convergence velocity produces a smoother growth of both ratios to final equilibrium conditions of 0.30 and 0.20 for the retrowedge and the prowedge, respectively. The low convergence velocity allows earlier attainment of the equilibrium conditions for both the prowedge (at 15% shortening) and retrowedge (at 30% shortening). Plots of distance of the deformation fronts

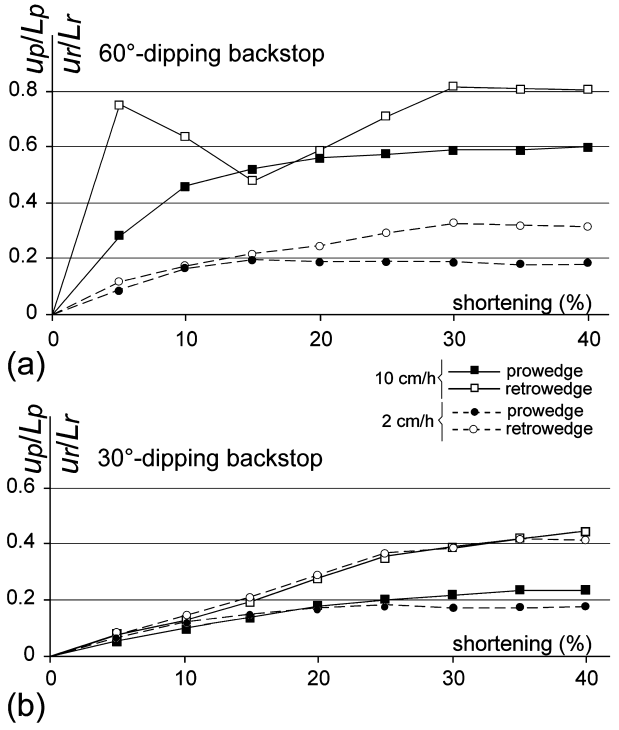

Fig. 7. Plots of u_p/L_p and u_r/L_r vs. % shortening for the different experimental configurations. Low-dipping backstop and low convergence velocities produce the lower ratios.

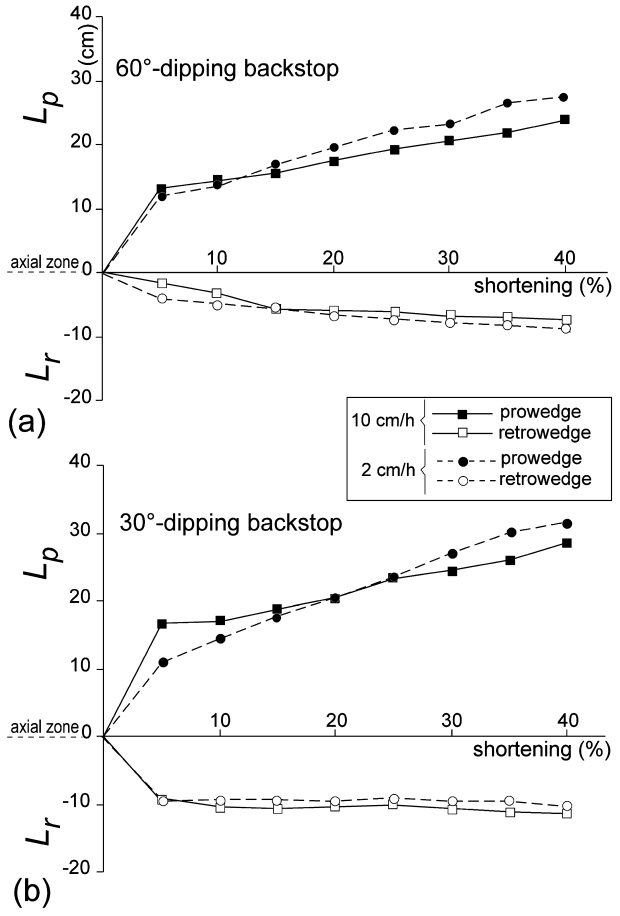

Fig. 8. Distance of the prowedge and retrowedge deformation fronts from the wedge axial region with increasing shortening (negative values toward the retrowedge). Prowedge deformation is favoured at low convergence velocity and for high-angle backstop.

from the axial zone indicate a wider deformed region for low convergence velocity in the prowedge and, in a lesser amount, in the retrowedge (Fig. 8). The ratio L_p/L_r shows that a constant ratio between the frontward and the retroward propagation of the deformation was attained with

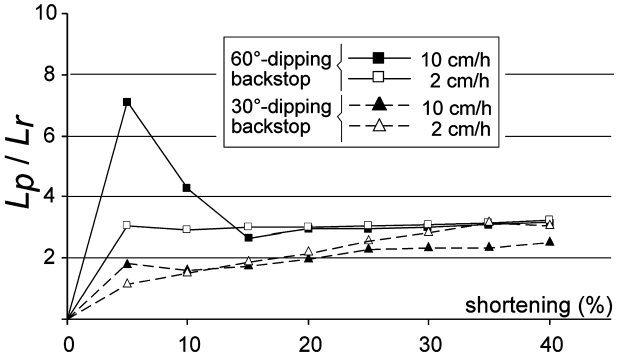

Fig. 9. Plots of L_p/L_r vs. % shortening for the different experimental configurations. Retrowedge deformation is favoured for flat-lying backstop and fast convergence velocity.

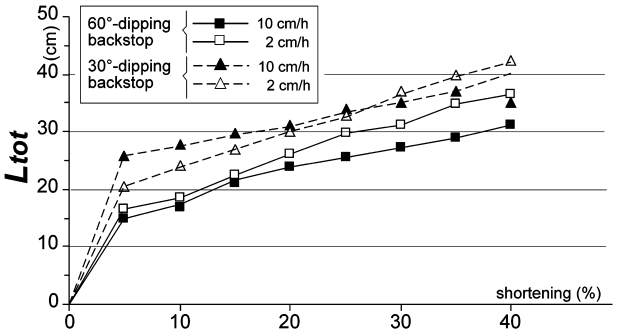

Fig. 10. Plots of L_{tot} vs. % shortening for the different experimental configurations. Flat-lying backstop and low convergence velocity configurations produce the wider deformed area.

increasing shortening for both the imposed convergence velocities (Fig. 9).

4.2. 30°-dipping backstop configuration (experiments W9803 and W9804)

Independently of the applied convergence velocity, an uplifted plug forms frontward of the subduction slot (Fig. 4). In both cases, the position of the wedge axial zone progressively migrates retroward with increasing shortening, and the migration is higher than that for the 60°-dipping backstop configuration (Fig. 5). Migration of the wedge axial zone is not influenced by the applied convergence velocity. The higher values of uplift in the axial region corresponds to fast convergence velocity, but uplift values are lower than those obtained for the 60°-dipping backstop configurations (Fig. 6). Plots of u_p/L_p and u_r/L_r ratios show a similar path for both convergence velocities (Fig. 7b). In the retrowedge, the u_r/L_r ratio continuously increases, attaining a nearly constant value (around 0.40) only for the slow convergence velocity and for shortening values higher that 30%. The u_p/L_p ratios show an early stage of growth, after which constant values are attained. Higher values characterise the fast convergence velocity (0.22 with respect to 0.18). Low convergence velocity allows earlier attainment of the equilibrium conditions for the prowedge: 20% shortening, compared with 30% shortening at fast convergence velocity. Plots of distance of the deformation front from the axial zone indicate a wider deformed region in the prowedge for lower convergence velocity and in the retrowedge region for higher convergence velocity, respectively (Fig. 8b). The L_p/L_r ratio clearly shows that lowering the convergence velocity produces an increase in the propagation of the prowedge deformation with increasing shortening (Fig. 9).

Summing up, the reduction of convergence velocity for a given backstop configuration produces the following features: (i) a decrease of the maximum uplift in the wedge axial regions; (ii) lower u_p/L_p and u_r/L_r ratios; and (iii) frontward propagation of the deformation front. For a given convergence velocity, decreasing the backstop dip has the following effects: (i) a smaller amount of uplift in the axial region of the wedge; and (ii) an increase in the growth size of retrowedge. Independently of the applied convergence velocity, lowering the backstop dip corresponds to a more intense retroward migration of the wedge axial region.

Variations of the parameter L_{tot} with increasing shortening for the different experimental configurations are shown in Fig. 10. The wider deformed areas are obtained for the lower convergence velocity and backstop dip.

5. Discussion

Both groups of models reveal the following similar features: (i) the development of an uplifted plug in the early stages of convergence (*sensu* Willett et al., 1993); (ii) the development of a doubly-vergent wedge with increasing convergence; and (iii) the increasing importance of the prowedge deformation mode in the later stages of convergence. The doubly-vergent geometry implies the occurrence of opposite shear senses during the wedge growth (Willett et al., 1993), which occur along the two main detachment surfaces consisting of the base plate (frontward-directed shear sense) and the top of the backstop (retroward-directed shear sense) for the prowedge and retrowedge, respectively. The final doubly vergent geometry is thus produced during continuous shortening without any change in the kinematic conditions. This general evolution is qualitatively comparable with those obtained in both sandbox (Malavieille, 1984; Byrne et al., 1993; Wang and Davis, 1996; Storti et al., 2000) and numerical (Willett et al., 1993) models.

In general terms, both prowedge and retrowedge (for slow convergence velocity) tend to attain a critical configuration with increasing shortening as in sand-box models with a similar experimental configuration (Wang and Davis, 1996), or with a deformable backstop (Storti et al., 2000). In our models, the stable configuration is a function of both backstop configuration and imposed convergence velocity. Slow convergence velocity and shallow-dipping backstop configuration produce lower aspect ratios (i.e. wider deformed areas) for both retrowedge and prowedge. When these data are compared with those obtained with a vertical backstop and the same experimental configuration (Rossetti et al., 2000), it is interesting to note that for the same convergence velocity the shallower backstop configurations produce the lower aspect ratios. Therefore, a more diffuse deformation is expected for shallow-dipping backstop and slow convergence velocity. The self-similar growth of the experimental wedges suggests that, as in the sandbox models of Wang and Davis (1996), and contrary to the constant-viscosity analogue model of Buck and Sokoutis (1994), no synorogenic extension (*sensu* Platt, 1986) occurs in the axial region. Syn-orogenic extension was also obtained in the constant-viscosity numerical models of Willett (1999), but only after significant growth. Thus, the

lack of extension in our models could be a consequence of temperature-dependent viscosity or of an upper limit to self-similar growth. The latter hypothesis remains to be explored by further experiments.

The backstop configuration and the convergence velocity have a fundamental influence on the deformation progression in the experimental wedges. Steeply dipping backstop configurations localise the axial region nearly above the subduction slot, whereas shallow-dipping backstop allows the retroward migration of the wedge axial region and the retroward propagation of the deformation front. The convergence velocity controls the amount and rate of outward migration of the deformation front for both the prowedge and retrowedge. The experimental results indicate that for shallow-dipping backstop the retrowedge deformation is favoured for fast convergence velocity, whereas for slow convergence velocity and steeply-dipping backstop the prowedge deformation is favoured. Thus, a decrease of the convergence velocity and/or an increase of the backstop dip angle can effect a change from prevalent hinterland- to foreland-vergent deformation. During the process, retrowedge and prowedge each evolve self-similarly.

These different modalities of wedge growth suggest, as expected, that the backstop geometry exerts a first-order control on the flow trajectories of the accreted material within the wedge. In steeply-dipping backstop configurations the material is forced to grow vertically, whereas in shallow-dipping backstop configurations the material is more efficiently translated retroward. These results are qualitatively comparable with those obtained in the sandbox models of Merle and Guiller (1989) and Bonini et al. (1999), suggesting that for steep backstop configurations vertical extrusion of accreted material occurs in the wedge axial region. Convergence velocity modulates the effects of the backstop configuration, controlling the velocity field within the growing orogenic wedge and the proportion between frontal accretion (prowedge deformation mode) and the retroward translation (retrowedge deformation mode) of the material incorporated in the wedge.

These results may have a fundamental importance in determining the evolution of convergent margins accreted against a rigid backstop, as it has been shown that the backstop configuration exerts an important control on the wedge axial zone location, residence time and trajectories of the material within the wedge. Different metamorphic grade distributions of rocks within natural wedges are in fact expected as a function of both backstop configuration and convergence velocity. In steeply-dipping backstop configurations, rocks transferred at the deep toe of the backstop can be more efficiently uplifted in the wedge axial region, as the rising wedge extrudes above the level of the confinement provided by the converging foreland and backstop (e.g. Bonini et al., 1999). This efficient uplift, when coupled with some exhumation mechanism, is consistent with the scenario for lower crustal metamorphic rocks unroofing proposed by Thompson et al. (1997). Conversely, in flat-lying backstop configurations, the same rocks are continuously translated retroward, resulting in assembly of material with different $P–T$ histories and generation of inverted metamorphic sequences in the retrowedge (e.g. Jamieson et al., 1996). Moreover, the difference in the wedge uplift patterns can enhance distinct concentrations of mechanical energy that could be extracted differently along the wedge profile when different boundary conditions are imposed (i.e. different convergence velocities and/or different backstop configurations). This can also enhance different surficial processes (erosion/sedimentation), not tested here, which have fundamental importance in the dynamical evolution of orogenic belts (e.g. Jamieson and Beaumont, 1988; Koons, 1990; Willett et al., 1993; Storti and McClay, 1995; Batt and Braun, 1997; Huerta et al., 1999).

6. Concluding remarks

The modelling technique described in this paper allows the study of the mechanical effects of a foreland-dipping rigid backstop and of convergence velocity on the large-scale evolution of viscous doubly-vergent orogenic wedges. Backstop geometry exerts a fundamental role in determining the shape and deformation style of model wedges. The convergence velocity controls the uplift in the wedge axial region and the amount of the outward migration of the deformation front in both the prowedge and retrowedge regions, influencing the foreland (prowedge) versus hinterland (retrowedge) style of the wedge growth.

Experimental wedges tend to grow in nearly self-similar, steady state conditions, with an aspect ratio depending upon the backstop dip and applied convergence velocity. Lower aspect ratios for both the prowedge and the retrowedge are obtained for lower convergence velocities and backstop dips. A more diffuse deformation is thus expected in natural orogens where accretion occurs against shallow-dipping backstop and at slow convergence velocities.

Acknowledgements

Models were financially supported by ENEL (Ente Nazionale Energia Elettrica). The authors wish to thank S. D'Offizi for his encouragement. F.R. is grateful to M. Luiselli for his important help during laboratory work at the ISMES laboratories. Discussions, comments and suggestions by F. Storti improved the paper. R. Funiciello co-ordinated this research. Thanks to O. Merle and S. Willett who provided helpful and thoughtful reviews. The work by G.R. is supported by a grant from NSERC (Natural Sciences and Engineering Research Council of Canada).

References

Adam, J., Reuter, C.-D., 2000. Crustal dynamics and active fault mechanics

during subduction erosion: application of frictional wedge analysis onto the North Chilean Forearc. Tectonophysics 321, 297–325.
Allemand, P., Lardeaux, J.-M., 1997. Strain partitioning and metamorphism in a deformable orogenic wedge: application to the Alpine belt. Tectonophysics 280, 157–169.
Argand, E., 1911. Les nappes de recouvrement des Alpes Pennines et leurs prolungements structuraux. Matériaux Carte géologique Suisse 31, 26.
Barr, T.D., Dahlen, F.A., 1989. Brittle frictional mountain building 2. Thermal structure and heat budget. Journal of Geophysical Research 94, 3923–3947.
Batt, G.E., Braun, J., 1997. On the thermomechanical evolution of compressional orogens. Geophysical Journal International 128, 364–382.
Beauchamp, W., Almendinger, R., Baranzaghi, M., Demnati, A., El Alji, M., Dahmani, M., 1999. Inversion tectonics and the evolution of the High Atlas Mountains, Morocco, based on a geological–geophysical transect. Tectonics 18, 163–184.
Beaumont, C., Quinlan, G., 1994. A geodynamic framework for interpreting crustal-scaleseismic-reflectivity patterns in compressional orogenes. Geophysical Journal International 116, 754–783.
Beaumont, C., Fullsack, P., Hamilton, J., 1994. Styles of crustal deformation in compressional orogens caused by subduction of the underlying lithosphere. Tectonophysics 232, 119–132.
Beaumont, C., Ellis, S., Pfiffner, A., 1999. Dynamics of sediment subduction–accretion at convergent margins: short-term modes, long-term deformation, and tectonic implications. Journal of Geophysical Research 104, 17573–17601.
Bonini, M., Sokoutis, D., Talbot, C., Boccaletti, M., Milnes, A.G., 1999. Indenter growth in analogue models of Alpine-type deformation. Tectonics 18, 119–128.
Braun, J., 1993. Three-dimensional numerical modeling of compressional orogenies: thrust geometry and oblique convergence. Geology 21, 153–156.
Buck, W.R., Sokoutis, D., 1994. Analogue model of gravitational collapse and surface extension during continental convergence. Nature 369, 737–740.
Byrne, D.E., Davis, D.M., Lynn, R.S., 1988. Loci and maximum size of thrust earthquakes and the mechanics of the shallow region of subduction zones. Tectonics 7, 833–857.
Byrne, D.E., Wang, W.H., Davis, D.M., 1993. Mechanical role of backstops in the growth of forearcs. Tectonics 12, 123–144.
Colletta, B., Letouzey, J., Pinedo, R., Ballard, J.-F., Balé, P., 1991. Computerized X-ray tomography analysis of sandbox models: examples of thin-skinned thrust systems. Geology 19, 1063–1067.
Dahlen, F.A., 1990. Critical taper model of fold-and-thrust belts and accretionary wedges. Annual Review of Earth and Planetary Sciences 18, 55–99.
Davis, D.M, 1996. Accretionary mechanics with properties that vary in space and time. In: Bebout, E., Scholl, D.W., Kirby, H.S., Platt, J.P. (Eds.), Subduction Top to Bottom, Geophysical Monograph 96, American Geophysical Union, Washington, pp. 39–48.
Davis, D., Suppe, J., Dahlen, F.A., 1983. Mechanics of fold-and-thrust belts and accretionary wedges. Journal of Geophysical Research 88, 1153–1172.
Davy, P., Gillet, P., 1986. The stacking of thrust slices in collision zones and its thermal consequences. Tectonics 5, 913–929.
Davy, P., Cobbold, P.R., 1991. Experiments on shortening of a 4-layer model of the continental lithosphere. Tectonophysics 188, 1–25.
Emerman, S., Turcotte, D.L., 1983. A fluid model for the shape of accretionary wedges. Earth and Planetary Science Letters 63, 379–384.
Escher, A., Beaumont, C., 1997. Formation, burial and exhumation of basement nappes at structural scale: a geometric model based on the western Swiss–Italian Alps. Journal of Structural Geology 19, 955–974.
Huerta, A.D., Royden, L.H., Hodges, K.V., 1999. The effects of accretion, erosion and radiogenic heat on the metamorphic evolution of collisional orogens. Journal of Metamorphic Geology 17, 349–366.
Jamieson, R.A., Beaumont, C., 1988. Orogeny and metamorphism: a model for deformation and pressure–temperature–time paths with application to the central and southern Appalachians. Tectonics 7, 417–445.
Jamieson, R.A., Beaumont, C., Hamilton, J., Fullsack, P., 1996. Tectonic assembly of inverted metamorphic sequences. Geology 21, 839–842.
Jolivet, L., Faccenna, C., Goffé, B., Mattei, M., Rossetti, F., Brunet, C., Storti, F., Cadet, J.P., Funiciello, R., D'Agostino, N., Parra, T., 1998. Midcrustal shear zones in post-orogenic extension: example from the Northern Tyrrhenian Sea (Italy). Journal of Geophysical Research 103, 12,123–12,160.
Kohlstedt, D.L., Evans, B., Mackwell, S.J., 1995. Strength of the lithosphere:constraints imposed by laboratory experiments. Journal of Geophysical Research 100, 17587–17602.
Koons, P.O., 1990. Two-sided orogen: collision and erosion from the sandbox to the Southern Alps, New Zealand. Geology 18, 679–682.
Koyi, H., 1995. Mode of internal deformation in sand wedges. Journal of Structural Geology 17, 293–300.
Lallemand, S., Malavieille, J., Calassou, S., 1992. Effects of oceanic ridge subduction on accretionary wedges: experimental modelling and marine observations. Tectonics 11, 1301–1313.
Malavieille, J., 1984. Modélisation expérimentale des chevauchements imbriqués: application aux châines des montagnes. Bulletin de la Société Géologique de France 7, 129–138.
Marshak, S., Wilkerson, M., 1992. Effect of overburden thickness on thrust belt geometry and development. Tectonics 11, 560–566.
Merle, O., Guiller, B., 1989. The building of the Swiss central Alps: an experimental approach. Tectonophysics 165, 41–56.
Molnar, P., Lyon-Caen, H., 1988. Some simple physical aspects of the support, structure and evolution of mountain belts. Geological Society of America, Special Paper 218, 179–207.
Mulugeta, G., 1988. Modelling the geometry of Coulomb thrust wedges. Journal of Structural Geology 10, 847–859.
Muñoz, J.A., 1992. Evolution of a continental collision belt: ECORS–Pyrenees crustal balanced cross-section. In: McClay, K. (Ed.). Thrust Tectonics. Chapman and Hall, New York, pp. 235–246.
Ord, A., Hobbs, B.E., 1989. The strength of the continental crust, detachment zones and the development of plastic instabilities. Tectonophysics 158, 269–289.
Pavlis, T.L., Bruhn, R.L., 1983. Deep-seated flow as mechanism for the uplift of broad fore arc ridges and its role in the exposition of high P/T metamorphic terranes. Tectonics 2, 473–497.
Peacock S.M., 1996. Thermal and petrologic structure of subduction zones. In: Bebout, E., Scholl, D.W., Kirby, H.S., Platt, J.P. (Eds.), Subduction Top to Bottom, Geophysical Monograph 96, American Geophysical Union, Washington, pp. 119–133.
Platt, J.P., 1986. Dynamics of orogenic wedges and the uplift of high-pressure metamorphic rocks. Geological Society of American Bulletin 97, 1037–1053.
Polino, R., Dal Piaz, G.V., Gosso, G., 1990. Tectonic erosion at the Adria margin and accretionary processes for the Cretaceous orogeny of the Alps. Memories Societè Geologique de France 156, 345–367.
Principi, G., Treves, B., 1984. Il sistema corso-appenninico come prisma diaccrezione. Riflessi sul problema generale del limite Alpi-Appennino. Memorie Società Geologica Italiana 28, 529–576.
Ranalli, G., 1995. Rheology of the Earth. 2nd ed. Chapman & Hall, London.
Ranalli, G., Murphy, D.C., 1987. Rheological stratification of the lithosphere. Tectonophysics 132, 281–295.
Rossetti, F., Ranalli, G., Faccenna, C., 1999. The rheology of paraffin as an analogue material for viscous crustal deformation. Journal of Structural Geology 21, 413–417.
Rossetti, F., Faccenna, C., Funiciello, R., Ranalli, G., Storti, F., 2001. Modeling the temperature-dependent strength in orogenic wedges: first results from a new thermomechanical apparatus. In: Koyl, H. A., Mancktelow, N. S. (Eds.). Tectonic modeling: A volume in honor of Hans Ramberg, Geological Society of America, Memoirs, 193, pp. 267–274.
Rossetti, F., Faccenna, C., Ranalli, G., Storti, F., 2000. Convergence rate-

dependent growth of viscous orogenic wedges. Earth and Planetary Science Letters 178, 367–372.

Royden, L., 1996. Coupling and decoupling of crust and mantle in convergent orogens: implications for strain partitioning in the crust. Journal of Geophysical Research 101, 17679–17705.

Schmidt, S.M., Pfiffner, A., Fritzheim, N., Schönborn, G., Kissing, E., 1996. Geophysical–geological transect and tectonic evolution of the Swiss–Italian Alps. Tectonics 15, 1036–1064.

Silver, E.A., Reed, D.L., 1988. Backthrusting in accretionary wedges. Journal of Geophysical Research 93, 3116–3126.

Stockmal, G.S., 1983. Modelling of large-scale orogenic wedge deformation. Journal of Geophysical Research 88, 8271–8287.

Storti, F., McClay, K., 1995. The influence of sedimentation on the growth of thrust wedges in analogue models. Geology 23, 999–1003.

Storti, F., Salvini, F., McClay, K., 2000. Synchronous and velocity-partitioned thrusting and thrust polarity reversal in experimentally produced, doubly-vergent thrust wedges: implications for natural orogens. Tectonics 19, 378–379.

Thomson, A.B., Schulman, K., Jezek, J., 1997. Extrusion tectonics and elevation of lower crustal metamorphic rocks in convergent orogens. Geology 25, 491–494.

Toboaga, A., Rovera, L.A., Fuenzalida, A., Cisternas, A., Hervé, P., Bijiward, H., Olaya, J., Rivera, C., 2000. Geodynamic of the northern Andes: subduction and intracontinental deformation (Colombia). Tectonics 19, 787–813.

Torrini, R., Speed, R.C., 1989. Tectonic wedging in the forearc basin-accretionary prism transition, Lesser Antilles forearc. Journal of Geophysical Research 94, 10549–10584.

Von Huene, R., Scholl, D.W., 1991. Observations at convergent margins concerning sediment subduction, subduction erosion, and the growth of continental crust. Review of Geophysics 29, 279–316.

Wang, C.-Y., Shi, Y.-L., 1984. On the thermal structure of subduction complexes: a preliminary study. Journal of Geophysical Research 89, 7709–7718.

Wang, W.H., Davis, D.M., 1996. Sandbox model simulation of forearc evolution and non-critical wedges. Journal of Geophysical Research 101, 11329–11339.

Willett, S., 1999. Rheological dependence of extension in wedge models of convergent orogens. Tectonophysics 305, 419–435.

Willett, S., Beaumont, C., Fullsack, P., 1993. Mechanical models for the tectonics of doubly vergent compressional orogens. Geology 21, 371–374.